ARTICLE

Structural and Magnetic Property of Ion Irradiated TiO_2 Single Crystals

Bin-feng Ding*, Feng-hua Xiang

Department of Physics and Electronic Information, Langfang Teachers College, Langfang 065000, China

(Dated: Received on July 1, 2011; Accepted on December 19, 2011)

Ferromagnetism is induced in pure TiO_2 single crystals by oxygen ion irradiation. The ferromagnetism is observed up to room temperature and is with weak temperature dependence. By combining X-ray diffraction, Rutherford backscattering/channelling, Raman scattering, and electron-spin resonance spectroscopy, supperconducting quantum interference device, displacement per atom, we measured the lattice damage accumulation with increasing fluences. A defect complex, *i.e.*, Ti^{3+} on the substitutional accompanied by oxygen vacancies, has been identified in the irradiated TiO_2. This kind of defect complex results in a local (TiO_{6-x}) stretching Raman mode. We elucidate that Ti^{3+} with one unpaired 3d electron provide the local magnetic moments.

Key words: Rutherford backscattering/channelling, Displacement per atom, Vacancy and interstitial

I. INTRODUCTION

Recently, ferromagnetism has been observed in nonmagnetically doped, but defective oxides, such as TiO_2 [1−4]. This kind of observation challenges the conventional understanding of ferromagnetism, due to spin-split statesor bands. Thus, one fundamental question must be answered: where are the moments located? Intensive theoretical works have been performed to understand the ferromagnetism in defective oxides [5−7]. In these works, the triplet states of p-like electrons, located at cation or oxygen vacancies, yield the local moments, leading to a kind of ferromagnetism without the involvement of 3d electrons. Experimentally the ferromagnetism in undoped TiO_2 has been found to relate with oxygen vacancies (O_V) [2, 3]; however, its mechanism remains unclear. It is worth noting that Ti^{3+} ions with one 3d electrons are usually generated in slightly reduced TiO_2. When O is removed, the excess electrons are unpaired [8]. They can occupy the nearby localized Ti3d orbit and therefore convert Ti^{4+} to Ti^{3+}. In a reduced rutile TiO_2(110) surface, such a defect complex, Ti^{3+}-O_V, has been well studied by first-principles calculations [9, 10] and experimentally by resonant photoelectron diffraction [11]. Therefore, experimental work is needed to clarify whether the magnetic moments in defective TiO_2 are due to unpaired 3d electrons localized on Ti^{3+}.

Ion irradiation is a nonequilibrium and reproducible method of inducing defects. Energetic ions displace atoms from their equilibrium lattice sites, thus creating mainly vacancies and interstitials. The amount of defects can be controlled by the ion fluence and energy. In this work, we irradiated rutile TiO_2 single crystals with 2 MeV O ions, resulting in a projected range of 1.52 μm and a longitudinal straggling of 0.16 μm as calculated by the stopping and range of ions in matter (SRIM) code [12]. As a result of this irradiation, the formation of Ti/O vacancies/interstitials is expected [12]. We selected high-energy oxygen ions as projectiles to avoid the introduction of foreign elements. Moreover, from a ballistic point of view, the creation of oxygen vacancies is more efficient, *e.g.*, by a factor of 1.5 larger than the Ti-vacancy creation. From SRIM calculations it is also evident that, at the given energy, the maximum atomic concentration of the implanted oxygen ions is by a factor of 500 smaller than the concentration of oxygen recoils. For the region of maximum defect creation, *i.e.*, at the end of the ion range, those projectiles play no chemical role. Thus, the desired local oxygen deficiency can be obtained by the proposed experimental procedure. The selection of TiO_2 single crystals instead of thin films is expected to exclude any effect of possible magnetic impurities in the underlying substrates [13] and of the interfaces between films and substrates [14].

II. EXPERIMENTS

Commercial rutile TiO_2 single crystals were irradiated with 2 MeV O ions at room temperature with fluences from 1×10^{15} cm^{-2} to 5×10^{16} cm^{-2}. All samples are from the same purchase charge with an equal size of 5 mm×5 mm×0.53 mm, corresponding to a mass of 53 mg. The samples thereafter were named as virgin, 1×10^{15}, 2.5×10^{15}, 5×10^{15}, 7.5×10^{15}, 1×10^{16}, 5×10^{16}. The samples were investigated us-

*Author to whom correspondence should be addressed. E-mail: ding_binfeng@126.com

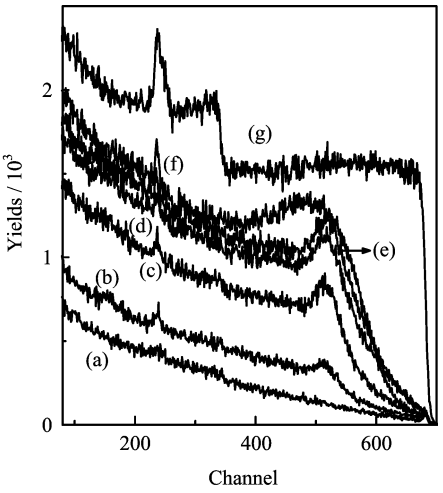

FIG. 1 RBS/channeling spectra for ion irradiation TiO_2 samples with different irradiation fluences. (a) Virgin, (b) 1×10^{15}, (c) 2.5×10^{15}, (d) 5×10^{15}, (e) 7.5×10^{15}, (f) 1×10^{16}, and (g) 5×10^{16}.

ing SQUID magnetometry (Quantum Design MPMS-7XL), XRD (Siemens D5005), Rutherford backscattering/channelling (RBS/C), displacement per atom (DPA), Raman spectroscopy (LabramHR, Jobin-Yvon-Horiba), and ESR (Bruker ELEXSYS E500 at 9.4 GHz). SQUID measurements indicate that the virgin TiO_2 single crystals are weak paramagnets with a susceptibility of 7.7×10^{-6} emu.

III. RESULTS AND DISCUSSION

A. Lattice damage

The lattice damage before and after O ion irradiation TiO_2 was evaluated by RBS/C spectra. The RBS/C spectra were collected with a collimated 1.7 MeV He^+ beam at a backscattering angle of 170°. The sample was mounted on a three-axis goniometer with a precision of 0.01°. The channeling spectra were collected by aligning the sample to make the impinging He^+ beam parallel with the TiO_2[110] axis. The DPA dependence of channelling is measured by RBS/C for 1×10^{15}. RBS/C result shows that the lattic defect is produced at TiO_2 surface 520 and 240 channelling by O ion irradiation, and experiment also shows that the Ti DPA is 12%. This certifies that vacancies and interstitials is produced excesively in pure TiO_2.

Figure 1 shows representative RBS/C spectra. In the channelling spectra, there are two peaks which mainly originate from the lattice disorder due to irradiation, namely, the sharp hump (the sharp peak) and the surface damage regions (the broad hump), respectively. The surface damage region is often a sink for ion-irradiation-induced point defects, while the sharp hump region is where the Ti^{x+} deposits. The lattice

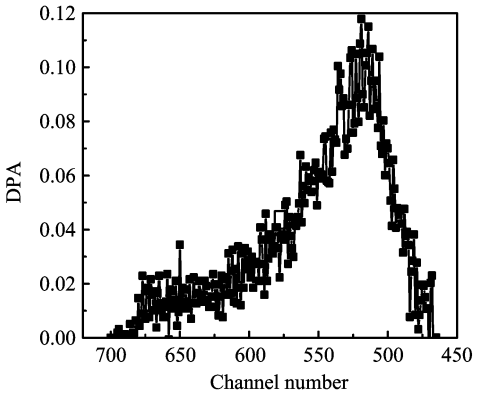

FIG. 2 Ti DPA curves dependence of channelling number for the ion irradiation TiO_2 sample with fluences of 10^{15} cm^{-2}.

damage gets larger with increasing ion-irradiation fluence, particularly, there is a enlarged peak at 240 and 520 (surface damage region) channelling number, it indicates that lattice disorder degree.

Figure 2 shows Ti DPA of the sample with fluence 1×10^{15} cm^{-2} versus channelling, the obvious peak at 520 channelling number, it certifies that the vacancies, interstitials and substitution in TiO_2 is very high, this is in better agreement with RBS/C experiment.

B. Magnetic property

Figure 3(a) shows the measured magnetic moment of TiO_2 at 300 K before and after irradiation with a fluence of 5×10^{15} cm^{-2}. After irradiation the sample shows a ferromagnetic hysteresis added to the linear paramagnetic background. The saturation magnetic moment is in the order of 10^{-5} emu, well above the sensitivity limit of SQUID magnetometry. Figure 3(b) shows the low-field part on an enlarged scale. The coercive field of around 10 mT can be clearly resolved. Figure 3(a) shows the irradiation-fluence-dependent magnetic moment of TiO_2 single crystals after subtracting the linear paramagnetic background. The magnetic moment first increases drastically with increasing fluence, but for the fluences above 5×10^{15} cm^{-2}, it decreases significantly again. For the 5×10^{15} sample, with the largest magnetic moment, we also measured the hysteresis loops at different temperatures (not shown). The loops are weakly temperature dependent. This is also a feature of the reported defect-induced ferromagnetism [15].

C. Structural property

The structural evolution upon ion irradiation was assessed by XRD, ESR and Raman-scattering measurements. Figure 4(a) shows the XRD patterns close to the TiO_2 (330) peak before and after irradiation at different

DOI:10.1088/1674-0068/25/01/19-24

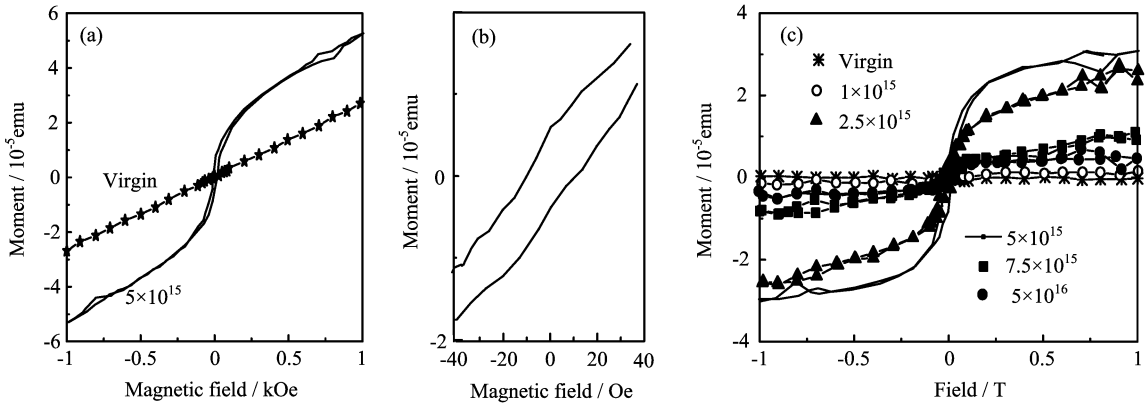

FIG. 3 (a) Magnetic moments measured at 300 K as a function of magnetic field before and after irradiation. (b) the low-field part of the loop for sample 5×10^{15}. (c) Magnetic moments at 300 K for samples with an equal sample size and different ion fluences. The linear paramagnetic background has been subtracted.

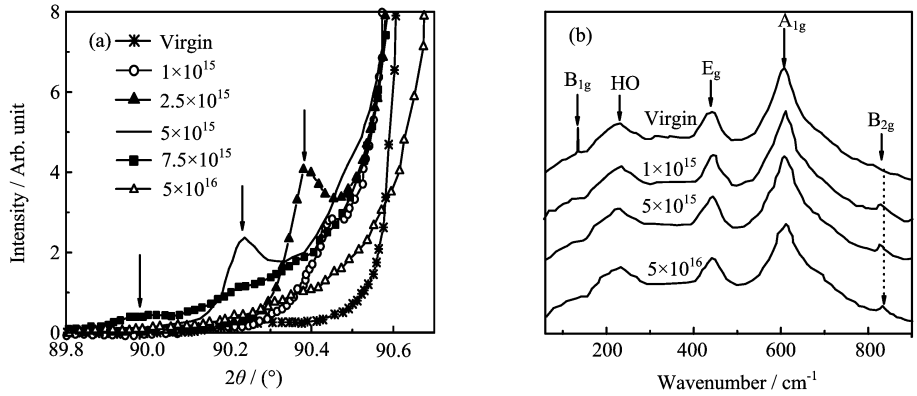

FIG. 4 (a) XRD pattern for O-irradiated TiO_2. The peaks (marked by arrows) in the left side of the TiO_2 (330) peak evidence the irradiation-generated strain in TiO_2. (b) Raman spectra of TiO_2 single crystals after oxygen ion irradiation with different fluences. The spectra are shifted vertically for better visualization. A clear mode at the range of B_{2g} (as indicated by the dashed arrow) has been observed after irradiation.

fluences. One remarkable characteristic is that a new peak appears at the left side of the (330) peak after irradiation. This new peak is induced by a strained TiO_2 layer with a larger lattice spacing compared to that of the virgin TiO_2. With increasing fluence, this peak shifts toward smaller 2θ angles and arrives at a minimum at a fluence of 7.5×10^{15} cm^{-2}. The largest strain is around 0.5%; however, the peak becomes weaker. With further increasing fluence, the peak finally disappears and develops into a gradual shoulder, which means the loss of crystalline long-range ordering of the irradiated layer. This phenomenon is usually due to the fact that density point defects accumulate and develop into extended defects, *e.g.*, dislocations. The lattice expansion upon ion irradiation is a common feature in semiconductors, *e.g.*, in GaN [16].

The effect of oxygen implantation on the structural properties of TiO_2 was further studied by Raman spectroscopy. The experiments were carried out in a micro-Raman 180° backscattering geometry. The scattering intensities were measured using vertical orientation of the crystal [001]-axis relative to the electric-field vector of the incoming laser. The spectrum of the virgin sample (Fig.4(b)) shows four distinct lines which are assigned to the B_{1g}(143 cm^{-1}), E_g(447 cm^{-1}), and A_{1g}(612 cm^{-1}) fundamental modes and to a higher order (HO) band around 234 cm^{-1} of rutile TiO_2 [17]. The fourth Raman-active fundamental mode with B_{2g} symmetry appears as a weak shoulder at 820 cm^{-1}. Neither the fingerprint lines from the anatase TiO_2 at 144 cm^{-1} nor those of Ti_2O_3 at 269 and at 347 cm^{-1} have been observed in the irradiated samples [18−20]. Already at the smallest fluence, the irradiation induces (i) the complete disappearance of B_{1g} and (ii) significant changes in the range of the B_{2g} mode, where instead of the shoulder at 820 cm^{-1} a clearly resolved line appears at 834 cm^{-1} indicated by the dashed arrows in Fig.4(b). The B_{1g} mode is very sensitive to the long-range order of TiO_2 crystals. It softens when applying high pressure and loses intensity much faster than the other fundamental modes [20]. Raman spectra of microcrystalline and nanocrystalline TiO_2 of 5 nm−2 μm

DOI:10.1088/1674-0068/25/01/19-24

average crystallite size did not show the B_{1g} mode as reported recently [21]. An important conclusion of the complete absence of B_{1g} is that the information depth of the Raman spectra is limited to the irradiated part of the sample. The integrated intensity of the line at 834 cm^{-1} is ∼5.5 times larger than that of the corresponding shoulder for a virgin TiO_2. In virgin TiO_2 the B_{2g} mode represents an antisymmetric (Ti−O) stretching vibration of the (TiO_6) octahedra (Ti ions are surrounded by six O ions) [21]. It is therefore sensitive to the short-range order and the bond strength in the crystal, *i.e.*, the local environment of the Ti ions. Since a reduction in the crystallite size usually causes redshifts of vibrational modes, the observed blueshift by 14 cm^{-1} of the B_{2g} mode cannot be explained by phonon confinement.

Furthermore, the line can neither be assigned to an IR-active nor assigned to a silent mode of rutile TiO_2 possibly activated due to a crystal-symmetry reduction [22−25]. The line at 834 cm^{-1} indicates a stronger bond between the Ti and the O atoms than that in the virgin rutile. One possible reason is the reduced coordination number of Ti ions resulting in TiO_{6-x} instead of TiO_6 since a lower coordination number leads to bond contraction and higher vibrational frequencies. This mechanism should in principle also affect the other Raman lines, particularly the A_{1g} mode. However, a possible high-energy shoulder would be easily hidden under the large scattering intensity of the main components. The localized origin of the mode at 834 cm^{-1} is also supported by the dependence of the Raman line parameters on implantation fluences. While the A_{1g} and E_g lines are broadened with increasing oxygen fluence due to irradiation-induced defects, the local (TiO_{6-x}) stretching mode shows a slight line narrowing. Therefore, we conclude that oxygen irradiation results in the local distortion of the overall TiO_6 coordination, which gives rise to a local (TiO_{6-x}) stretching mode in the range of the B_{2g} mode. Such a distorted TiO_{6-x} octahedral has also been considered in a recent experimental and molecular dynamics simulation study of ion irradiation damage in TiO_2 [26].

In order to understand the origin of the local moments, ESR measurements were performed on the virgin and two selected irradiated samples: 5×10^{15} (with the largest magnetic moment) and 5×10^{16} (with the largest irradiation fluence). ESR directly probes the interaction between the unpaired electrons and the magnetic field. In a broad applied field range of 50−550 mT along the TiO_2 [001] axis and with temperatures down to 5 K, we only detected one ESR peak at a g factor of 1.9408 accompanied by a complicated hyperfine interaction pattern for the two irradiated samples. Figure 5 shows the featured field range of the measured ESR spectrum at 5 K for sample 5×10^{15}. Note that electrons trapped by vacancies have a g factor slightly larger than 2 and exhibit no hyperfine features [27, 28]. The line shape (see Fig.6 and Fig.7 for details) and the g factor are typical features in the so-called A spectrum due to Ti^{3+} [29, 30]. Now we come to the question: how are the Ti^{3+} generated after irradiation? Among the defects created by irradiation, only O vacancies and Ti interstitials can contribute excess electrons [8, 31]. There are three factors favoring the formation of Ti^{3+}-O_V defect complexes: (i) as the nearest-neighbor O vacancies are more close to substitutional Ti ions, (ii) the number of O vacancies is 1.5 times larger than that of Ti interstitials [12] and (iii) energetically the formation of O vacancies is slightly favored over the formation of Ti interstitials [8]. Therefore we can conclude that each of irradiation-induced oxygen vacancies leaves two electrons and converts the neighboring Ti^{4+} to Ti^{3+}, resulting in Ti^{3+}-O_V defect complexes. Such a converting in the reduced TiO_2 (110) surface has been confirmed recently by both theoretical and experimental works [10, 11]. It is important to note that the virgin sample shows no detectable ESR line down to 5 K (not

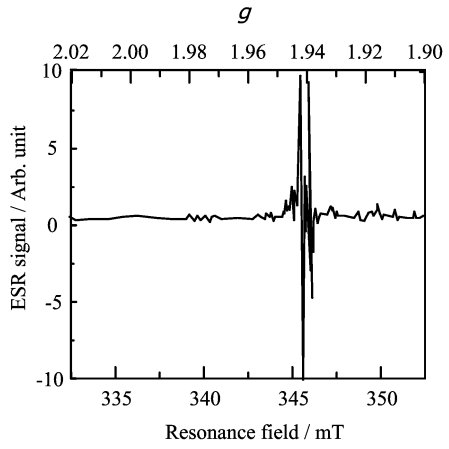

FIG. 5 ESR signals observed in sample 5×10^{15} at 5 K. The applied field is along the [001] axis. The main ESR peak accompanied by a hyperfine interaction pattern has a g factor of 1.9408.

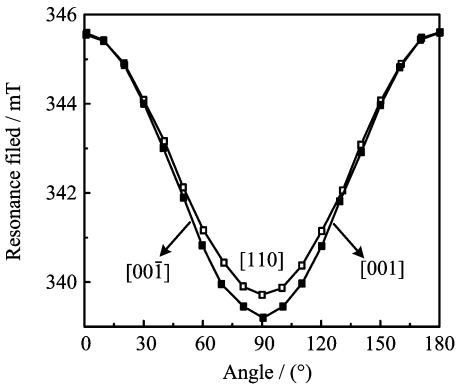

FIG. 6 Angular-dependent resonance field of the ESR spectrum: it is split into two lines upon field orientation changing from the [001]([00$\bar{1}$]) to the [110] axes. Open box: [110] and solid box: [001] and [00$\bar{1}$].

DOI:10.1088/1674-0068/25/01/19-24

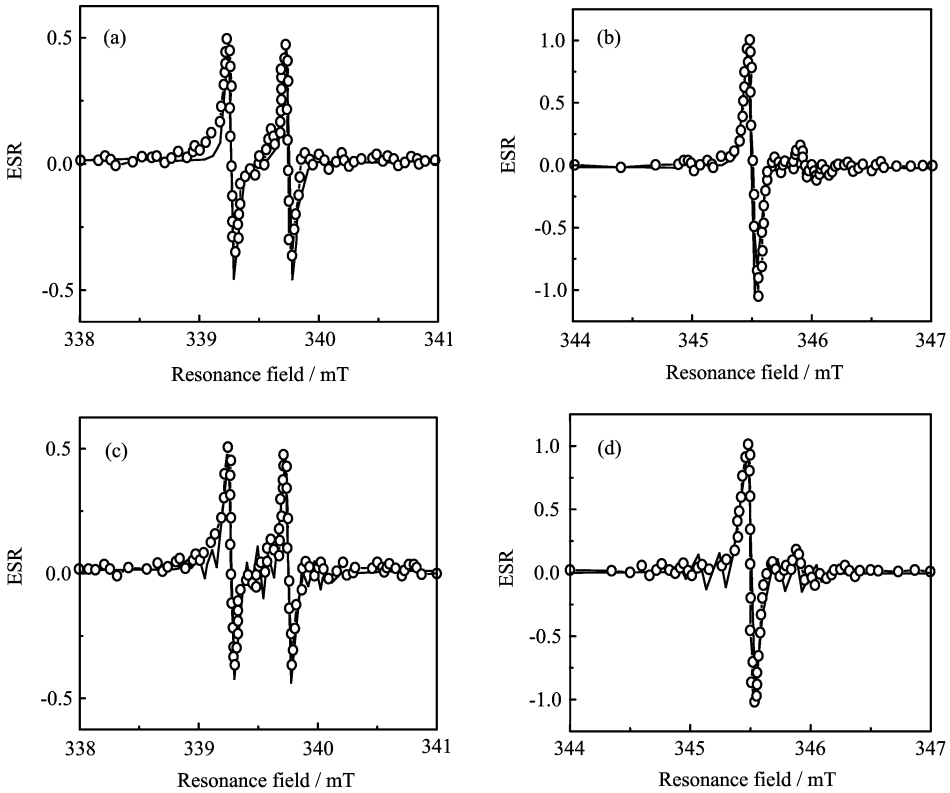

FIG. 7 Comparison between simulated (solid lines) and measured (open circles) ESR data. (a) and (c): with field along the [110] direction without (a) and with (c) considering hyperfine interaction. (b) and (d): with field along the [001] direction without (b) and with (d) considering hyperfine interaction.

shown) since the virgin TiO_2 contains no unpaired electrons [32, 33]. The site occupation of the Ti^{3+}, namely, substitutional or interstitial, is determined by the angular dependence of the A spectrum. The crystalline symmetry results in a twofold splitting of the Ti^{3+} ESR lines at substitutional sites and a fourfold splitting at interstitial sites, when the field orientation changed from the [001] to the [110] axes [30]. As shown in Fig.6, we can conclude that the Ti^{3+} in our samples occupy substitutional sites. We performed a simulation of the ESR spectra with this assumption as shown in Fig.7. For fields along [110] and [001] and with the anisotropic g factors $[g_x, g_y, g_z]$=[1.9766, 1.9738, 1.9408], we obtained the spectra as shown in Fig.7 (a)−(c). Without considering the hyperfine interaction, the simulated spectra agree reasonably well with the experimental data in g factor, line shape, and splitting with field rotation. When taking the hyperfine interaction into account, namely, the nuclear spin of ^{47}Ti(I=5/2) and ^{49}Ti(I=7/2), the simulations reproduce the experimental results even much better.

The presence of Ti^{3+} at substitutional sites also explains the XRD results considering the fact that substitutional Ti^{3+} are larger than Ti^{4+} resulting in the observed lattice expansion. However, the other point defects, *i.e.*, Ti/O interstitials, can also result in the lattice expansion. Combining the findings of Raman and ESR measurements, we conclude in the following. Among the various defects created by oxygen ion irradiation, Ti^{3+} on substitutional sites are accompanied by oxygen vacancies (O_V) forming defect complexes, which result in a local (TiO_{6-x}) stretching Raman mode. When the ion fluence is very large, the irradiated layer loses its long-range crystalline ordering so that the fundamental mode of TiO_2 is broadened.

IV. CONCLUSION

In this work, (i) a Ti^{3+}-O_V defect complex is generated due to ion irradiation. The Ti^{3+} provide local 3d moments which are decisively related with the observed ferromagnetism. (ii) There is an optimum fluence to produce enough Ti^{3+} while keeping the crystalline ordering. (iii) The amount of defects complex can be controlled by appropriate ion fluence and appropriate energy.

V. ACKNOWLEDGMENTS

The work was supported by the National Natural Science Foundation of China (No.50802041 and No.50872050), the National Basic Research Program of

DOI:10.1088/1674-0068/25/01/19-24

China (No.2011CB831524), the 2009 Self-Raised Funds Project of Langfang Science and Technology Bureau (No.2009013056), and the 2011 Key Project of the Langfang Teachers College (No.LSZZ201101).

[1] J. M. D. Coey, M. Venkatesan, P. Stamenov, C. B. Fitzgerald, and L. S. Dorneles, Phys. Rev. B **72**, 024450 (2005).
[2] S. D. Yoon, Y. Chen, A. Yang, T. L. Goodrich, X. Zuo, D. A. Arena, K. Ziemer, C. Vittoria, and V. G. Harris, J. Phys.: Condens. Matter **18**, L355 (2006).
[3] N. H. Hong, J. Sakai, N. Poirot, and V. Brizé, Phys. Rev. B **73**, 132404 (2006).
[4] S. Zhou, K. Potzger, G. Talut, H. Reuther, K. Kuepper, J. Grenzer, Q. Xu, A. Mücklich, M. Helm, J. Fassbender, and E. Arenholz, J. Phys. D **41**, 105011 (2008).
[5] I. S. Elfimov, S. Yunoki, and G. A. Sawatzky, Phys. Rev. Lett. **89**, 216403 (2002).
[6] J. Osorio-Guillén, S. Lany, S. V. Barabash, and A. Zunger, Phys. Rev. Lett. **96**, 107203 (2006).
[7] T. Chanier, I. Opahle, M. Sargolzaei, R. Hayn, and M. Lannoo, Phys. Rev. Lett. **100**, 026405 (2008).
[8] G. U. von Oertzen and A. R. Gerson, J. Phys. Chem. Solids **68**, 324 (2007).
[9] P. J. D. Lindan, N. M. Harrison, M. J. Gillan, and J. A. White, Phys. Rev. B **55**, 15919 (1997).
[10] G. U. Von Oertzen and A. R. Gerson, Int. J. Quantum Chem. **106**, 2054 (2006).
[11] P. Krüger, S. Bourgeois, B. Domenichini, H. Magnan, D. Chandesris, P. Le Fèvre, A. M. Flank, J. Jupille, L. Floreano, A. Cossaro, A. Verdini, and A. Morgante, Phys. Rev. Lett. **100**, 055501 (2008).
[12] J. Ziegler, J. Biersack, and U. Littmark, *The Stopping and Range of Ions in Matter*, New York: Pergamon, 132 (1985).
[13] F. Golmar, A. M. M. Navarro, C. E. R. Torres, F. H. Sánchez, F. D. Saccone, P. C. dos Santos Claro, G. A. Benítez, and P. L. Schilardi, Appl. Phys. Lett. **92**, 262503 (2008).
[14] A. Brinkman, M. Huijben, M. Van Zalk, J. Huijben, U. Zeitler, J. C. Maan, W. G. Van der Wiel, G. Rijnders, D. H. A. Blank, and H. Hilgenkamp, Nature Mater. **6**, 493 (2007).
[15] G. Kopnov, Z. Vager, and R. Naaman, Adv. Mater. **19**, 925 (2007).
[16] C. Ronning, E. P. Carlsonb, and R. F. Davis, Phys. Rep. **351**, 349 (2001).
[17] S. P. S. Porto, P. A. Fleury, and T. C. Damen, Phys. Rev. **154**, 522 (1967).
[18] T. Ohsaka, F. Izumi, and Y. Fujiki, J. Raman Spectrosc. **7**, 321 (1978).
[19] A. Mooradian and P. M. Raccah, Phys. Rev. B **3**, 4253 (1971).
[20] G. A. Samara and P. S. Peercy, Phys. Rev. B **7**, 1131 (1973).
[21] V. Swamy, B. C. Muddle, and Q. Dai, Appl. Phys. Lett. **89**, 163118 (2006).
[22] V. Maroni, J. Phys. Chem. Solids **49**, 307 (1988).
[23] W. Zhu, G. Z. Wang, X. Hong, and X. S. Shen, Chin. J. Chem. Phys. **24**, 91 (2011).
[24] P. Xiao, L. Li, Y. H. Zhang, H. F. Dai, Y. Z. Hu, and L. Lu, Chin. J. Chem. Phys. **23**, 113 (2010).
[25] S. L. Chen, H. T. Su, H. Chang, C. S. Jwo, and H. J. Feng, Chin. J. Chem. Phys. **23**, 231 (2010).
[26] G. R. Lumpkin, K. L. Smith, M. G. Blackford, B. S. Thomas, K. R. Whittle, N. A. Marks, and N. J. Zaluzec, Phys. Rev. B **77**, 214201 (2008).
[27] M. Sterrer, E. Fischbach, T. Risse, and H. J. Freund, Phys. Rev. Lett. **94**, 186101 (2005).
[28] S. V. Chong, K. Kadowaki, J. Xia, and H. Idriss, Appl. Phys. Lett. **92**, 232502 (2008).
[29] P. F. Chester, J. Appl. Phys. **32**, 2233 (1961).
[30] E. Yamaka and R. G. Barnes, Phys. Rev. **135**, A144 (1964).
[31] J. He, R. K. Behera, M. W. Finnis, X. Li, E. C. Dickey, S. R. Phillpot, and S. B. Sinnott, Acta Mater. **55**, 4325 (2007).
[32] M. Saleem, S. A. Siddiqi, S. Atiq, M. S. Anwar, and S. Riaz, Chin. J. Chem. Phys. **23**, 469 (2010).
[33] S. M. Ramay, S. A. Siddiqi, S. Atiq, M. S. Awan, and S. Riaz, Chin. J. Chem. Phys. **23**, 591 (2010).

DOI:10.1088/1674-0068/25/01/19-24